ACS APPLIED MATERIALS & INTERFACES

Letter

www.acsami.org

Highly Monodispersed Tin Oxide/Mesoporous Starbust Carbon Composite as High-Performance Li-Ion Battery Anode

Jiajun Chen*,† and Kazuhisa Yano*,†,‡

†Toyota Research Institute of North America, 1555 Woodridge Avenue, Ann Arbor, Michigan 48105, United States

‡Toyota Central R&D Laboratories, Nagakute, Aichi 480-1192, Japan

Supporting Information

ABSTRACT: The widespread commercialization of today's plug-in hybrid and all electric vehicles will rely on improved lithium batteries with higher energy density, greater power, and durability.To take advantage of the high density of SnO_2 anodes for Li ion batteries, we achieved a smart design of monodispersed SnO_2/MSCS composite with very high content of SnO_2 by a simple infiltration procedure. The synergistic effects of the unique nanoarchitecture of MSCS and the ultrafine size of SnO_2 nanoparticle endowed the composite with superior electrochemical performance. Because of the high density of the composite resulting from its monodispersed submicrometer spherical morphology, an exceptionally high reversible lithium storage capacity (both gravimetric and volumetric), very close to the theoretical capacity (1491 mA h/g), can be achieved with good cyclability (capacity retention of 92.5% after 15 cycles). The SnO_2/MSCS composite anode exhibited a high reversible average capacity of about 1200 mAh/g over 30 cycles at a current of 80 mAh/g, which corresponds to about 1440 mAh/cm^3 (practical volumetric capacity). In addition, a Coulombic efficiency close to 100% was achieved, and less than 25% first irreversible capacity loss was observed.

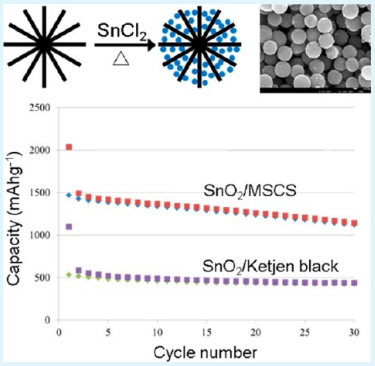

KEYWORDS: *lithium-ion battery, tin anodes, starburst carbon, monodispersed*

1. INTRODUCTION

Among the current commercial rechargeable battery technologies, lithium-ion battery technology offers the highest energy density and has dominated the market for mobile electronic devices for decades.[1−3] However, alternative forms of transportation, such as plug-in hybrid electric vehicles (PHEV) and all-electric vehicles (EV), require significant improvements in many perspectives, such as energy density, durability, and cost. To further increase the energy density, new electrode materials with higher specific and volumetric capacity are required. Compared with currently used commercial graphite anodes, tin-based anodes offer much higher specific gravimetric and volumetric capacity. Unfortunately, this class of materials are generally plagued by huge volume expansion (up to 360%) during lithiation, which generates enormous mechanical stress and pulverizes the electrode during the electrochemical charge/discharge cycles. The bulk tin electrode typically fails after only a few discharge/charge cycles.[4] SONY recently commercialized the Nexelion battery, which is based on a novel nanostructured anode, that contains nanosized amorphous SnCo embedded in carbon. However, the capacity of this anode is limited to 600 mA h/g.[5] Besides the pulverization problem of SnO_2 particles during cycling, agglomeration of primary particles drastically reduces the surface-to-volume ratio and diminishes the electrochemical activity of SnO_2. Over the years, extensive efforts have been devoted to addressing these issues by synthesizing nanoparticles or nanostructures with different morphologies (e.g., nanomaterials with hollow structure for providing the "breadth" space).[6,7] SnO_2, especially bare SnO_2 nanoparticles, also suffer from huge first irreversible capacity loss, which can be as high as 70%.[8,9]

Very recently, dispersed or decorated SnO_2 nanoparticles on graphene and/or carbon nanotubes (CNT) have been extensively investigated and reported for improved electrochemical performance and cyclability.[10−18] For instance, Paek et al. fabricated graphene nanosheets (GNS)/SnO_2 hybrid electrodes with 40% graphene.[10] At a current density of 50 mA/g, the charge capacity of SnO_2-GNS remained 570 mA h/g after 30 cycles; however, with only 40% Coulombic efficiency of first cycle. Golberg et al. fabricated N-doped graphene−SnO_2 sandwich paper, which enhanced electrochemical performance.[11] However, more than 68 wt % of carbon content (graphene) was needed for the composite. Li et al. decorated GNS with SnO_2 by utilizing atomic layer deposition (ALD).[12] Despite the improved performance, both crystalline and amorphous SnO_2−GNS composites were plagued by a large irreversible capacity loss in the first cycle. The Coulombic efficiency was 57.4 and 49%, respectively. Wang et al. prepared a SnO_2−graphene nanocomposite using a ternary self-assembly approach.[13] The nanocomposite (60 wt % SnO_2 and 40 wt % graphene) showed stable reversible capacity of 520 mA h/g at a current of 10 mA/g. Unfortunately, the intrinsic properties of

Received: June 5, 2013
Accepted: August 15, 2013
Published: August 15, 2013

graphene results in very low tap density of the composite electrodes. In addition, an extensive literature search revealed a high content of graphene, up to 70% may be required in composite electrodes. The situation with carbon nanotubes is similar, as they have large central cavities that also dramatically reduce the tap density. In situ formation of highly crystalline $LiFePO_4$ within a homogeneously dispersed conductive percolation network only requires 5−6% of multiwall carbon nanotubes (MWCNT).[19,20] To enhance the electrical conductivity and prevent agglomeration of SnO_2 nanocrystals, a much higher ratio of carbon nanotubes to cathode material ($LiFePO_4$) is required. Yang and Amine et al. developed a strategy in which SnO_2 nanocrystals were deposited on MWCNT. Regrettably, the composite was composed of 53 wt % CNT and an irreversible capacity loss of 50% was observed during the first cycle.[21] Noerochim et al.[22] reported CNT/SnO_2 anode papers (34 wt % SnO_2) that had a capacity of 454 mA h/g for 100 cycles at a current of 25 mA/g with a first cycle columbic efficiency of 38%. The low loadings and tap densities of these active materials significantly limits the practical volumetric energy density of the Li ion battery. Unfortunately, all the above strategies (decreasing particle size, accommodation by hollow structure or dispersing/decorating SnO_2 onto graphene/CNT), have the disadvantage of reducing the overall energy density of the anodes. A very effective approach to address this challenge is to disperse Sn or SnO_2 nanoparticles within a carbon matrix with nanospaces. The carbon matrix, while maintaining in its core a collection of nanosized particles, helps in containing the volume stress, and supplies an overall compact structure that ensures stability and provides high tap density. Unfortunately, previously developed fabrication techniques are only able to achieve 50 wt % Sn embedded in a carbon matrix,[23,24] thus leading to a relatively low capacity of 500 mA h/g.

In general, spherical particles exhibit less void space when packed compared to irregular particles. Hence, spherical particles are assumed to have a high tap density.[25−27] In many cases, to further increase the tap density, particles with identical size (monodispersity) are helpful. As a result, SnO_2 encapsulated monodispersed carbon spheres may provide a significant advantage. This is because the spherical morphology is beneficial in terms of the enhanced tap density of the composite, which is essential to the practical application in lithium ion batteries. In the present work, we developed a strategy employing monodispersed starburst carbon spheres (MSCS), which have high monodispersity and high specific surface as a host for SnO_2.[28,29] The synthesized highly monodispersed SnO_2/MSCS composite contains very high SnO_2 content (80% SnO_2 by weight). The submicrometer monodispersed mesoporous spherical morphology results in high density of the composite electrodes with a mass loading of active material of about 3 mg/cm^2. We demonstrated the performance of SnO_2/MSCS as an anode with extremely high capacity during initial cycles and a high reversible gravimetric capacity of 1200 mA h/g at a current of 80 mA/g over 30 cycles, which corresponds to a volumetric capacity about 1440 mA h/cm^3. The encapsulated SnO_2 has minimal side reactions with the electrolyte leading to high columbic efficiency (73%) and low irreversible capacity (less than 25%) for the first cycle. To the best of our knowledge, this is the first report concerning SnO_2 anodes with the combination of exceptional capacity (both gravimetric and volumetric) and high Coulombic efficiency.

2. RESULTS AND DISCUSSION

SnO_2/MSCS and SnO_2/ketjen black (SnO_2/KB) materials were prepared by an infiltration procedure. To facilitate the incorporation of SnO_2, the surface of MSCS was modified by heating in air at 400 °C. The surface of the oxidized MSCS was composed of significantly more oxygen-containing moieties, i.e., hydroxyls, quinones, and carboxylic acids (C−OH, C═O, C—OOH), which could be beneficial for loading SnO_2 nanoparticles.[30] To ensure the crystallization of SnO_2 occurred without loss of carbon, we annealed both composites under Ar atmosphere. The crystal structure of the SnO_2 was examined using X-ray diffraction (XRD) as shown in Figure 3a.There is a

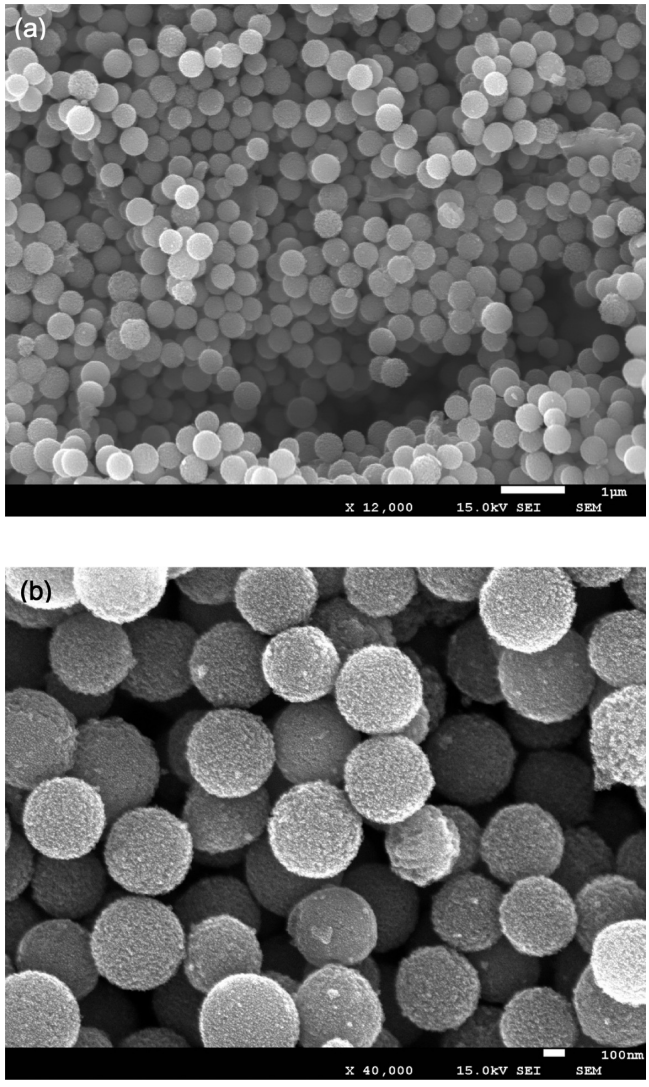

Figure 1. SEM images of the SnO_2/ MSCS composite.

considerably broadened peak which was clearly indexed as tetragonal SnO_2 (JCPDS PDF No. 41−1445, space group: $P4_2/mnm$). The lattice parameters of SnO_2 in SnO_2/MSCS were $a = b = 4.734(1)$ Å, $c = 3.193(1)$ Å. The lattice parameters of SnO_2 in SnO_2/KB were $a = b = 4.737(1)$ Å, $c = 3.199(2)$ Å. Both are in fair agreement with the mineral structure Cassiterite from Bolzan et al.[31] The broad peaks in the pattern of the material are evidence of the small primary particle size of SnO_2. The crystalline size of SnO_2 estimated by means of the Scherrer equation was about 3.5 nm.

dx.doi.org/10.1021/am4021846 | ACS Appl. Mater. Interfaces 2013, 5, 7682−7687

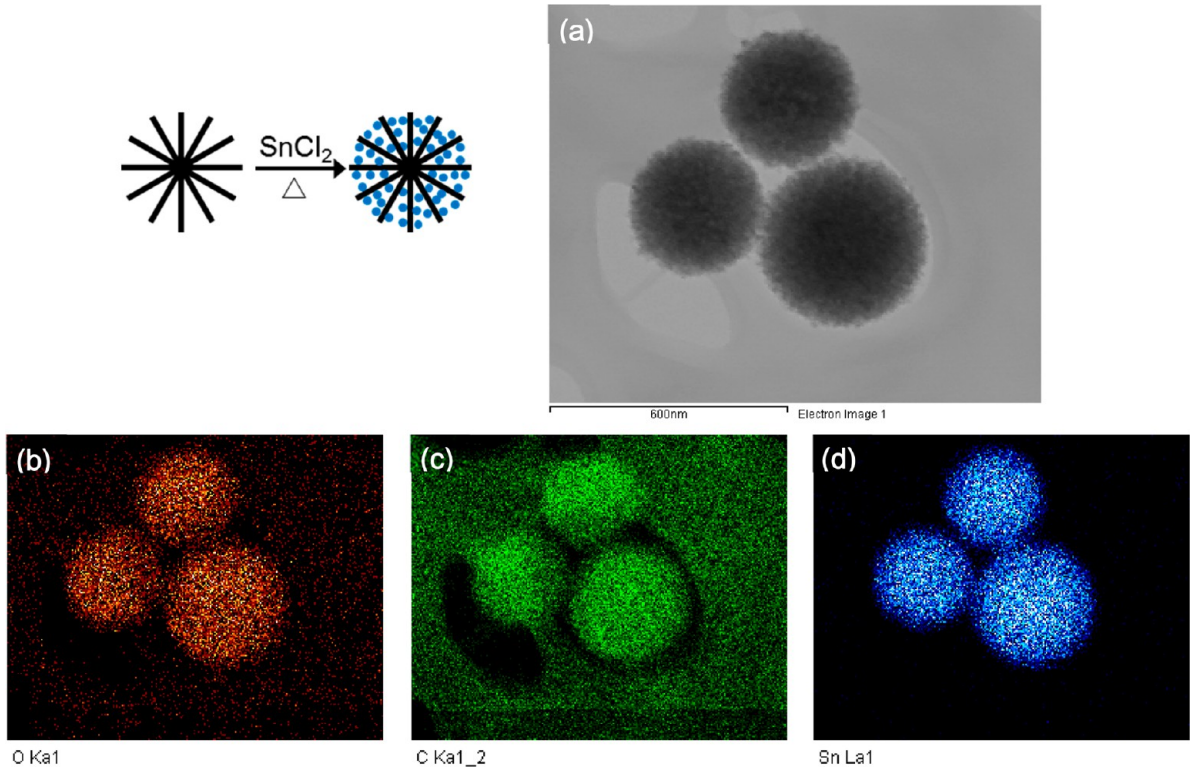

Figure 2. Schematic illustration of formation of SnO_2/ MSCS composite, and (a–d) elemental mapping images of SnO_2/ MSCS composite.

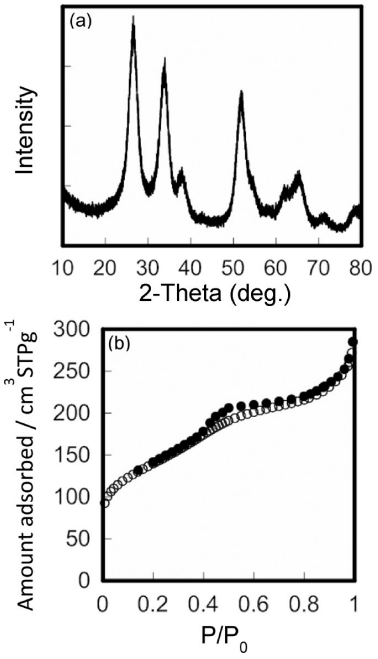

Figure 3. (a) XRD pattern of SnO_2/MSCS composite. (b) N_2 adsorption–desorption isotherms for SnO_2/MSCS composite.

Previous attempts to fill sufficient SnO_2 particles into mesoporous carbon spheres were unsuccessful. Gerbaldi et al. reported SnO_2 loadings as low as 30 wt % and an irreversible capacity loss of 65% was observed during the first cycle.[32] Compared to the standard low loading of about 40% in carbon nanotubes or graphene, a very large amount of SnO_2 can be incorporated into MSCS. Combustion Infrared Detection of carbon content in the composites are 21 and 23 wt % for SnO_2/MSCS and SnO_2/KB, respectively. Thus, a high loading of about 80 wt % SnO_2 was achieved by infiltration of $SnCl_2$ into both MSCS and KB. Figure 1 shows SEM images of typical SnO_2/MSCS. The average diameter estimated from SEM is 387 nm with a 7.6% coefficient of variation. The TEM clearly shows that the isolated SnO_2 nanoparticles, which are about 3–5 nm in size, are homogenously dispersed inside MSCS. As shown in Figure 2, elemental mapping of the SnO_2/MSCS reveal uniform distribution of Sn, O, and C and further indicates the homogeneous dispersion of SnO_2 nanoparticles throughout the MSCS structure. TEM images of the original MSCS and SnO_2/MSCS composite are shown in the Supporting Information, Figure S1. The original MSCS is quite transparent; however, once the heavy Sn element is incorporated, the composite is dark. The Brunauer–Emmett–Teller (BET) specific surface area of SnO_2/KB and SnO_2/MSCS composites are about 375 and 489 m^2/g, respectively. The pore size of SnO_2/MSCS is similar to the original MSCS, which is about 3.9 nm. This indicates the SnO_2/MSCS composite has a well-preserved MSCS mesoporous feature after infiltration of SnO_2 into MSCS pores.[33] If we assume all of SnO_2 nanoparticles (~80 wt % determined by Combustion Infrared Detection) are confined in mesopores, about 60% of pores are expected to be filled with SnO_2. As expected, we observed the decrease of pore volume after infiltration of SnO_2 into MSCS. The total pore volume of SnO_2/MSCS is about 0.39 cm^3/g which is about 40% of the original MSCS (0.92 cm^3/g) pore volume. Thus, we can conclude SnO_2 nanoparticles are fully incorporated in the starburst carbon spheres. The result also agrees well with homogeneous distribution of Sn by elemental mapping.

MSCS are composed of radially aligned nanorods and the nanopores in SnO_2/MSCS could act as buffering spaces against the volume change of SnO_2 nanoparticles during cycling. In addition, these carbon nanorods could also play an important

role for immobilizing the SnO_2 nanoparticles preventing agglomeration.The unique structure of SnO_2/MSCS motived us to investigate its electrochemical properties. The discharge/charge performances of these two composites were conducted at a current density of 80 mA/g and shown in Figure 4. The electrochemical performance of SnO_2/KB was evaluated as a control experiment. The reaction mechanism of SnO_2 with lithium has been proposed as the following two steps

$$SnO_2 + 4Li^+ + 4e^- \rightarrow Sn + 2Li_2O \quad (1)$$

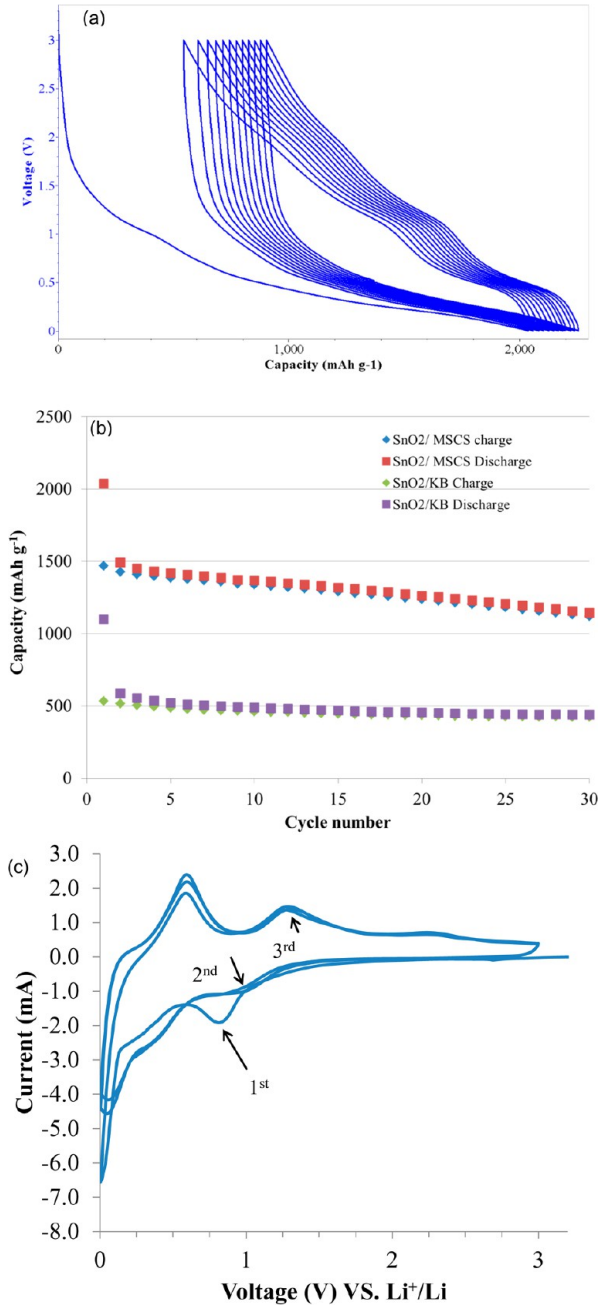

Figure 4. (a) Electrochemical performance of the SnO_2/MSCS composite at a constant current density of 80 mA/g. (b) Comparison of the electrochemical properties of SnO_2/MSCS composite and SnO_2/ Ketjenblack carbon composite at the same current density of 80 mA/g. (c) CV profiles of SnO_2/MSCS showing the first three cycles between 5 mV and 3 V at a scanning rate of 0.1 mV s^{-1}.

$$Sn + xLi^+ + xe^- \leftrightarrow Li_xSn\ (0 \le x \le 4.4) \quad (2)$$

In the first step, SnO_2 is reduced to metallic Sn, which was previously believed to be only partially reversible. The second process is the Sn alloying/dealloying reaction with lithium, which is very reversible in most cases. If this reaction is completely reversible, the overall electrochemical processes could lead to the insertion of a total of 8.4 Li-ions per formula unit of SnO_2. This corresponds to a theoretical capacity of 1491 mA h/g. Very recent findings shows a highly reversible conversion reaction followed by an alloying/dealloying reaction can lead to a much higher capacity than the previous reported maximum of 781 mA h/g.[12,15]

In spite of nearly the same loading and particle size of ultrafine SnO_2 (less than 5 nm) in both SnO_2/MSCS and SnO_2/KB composites, a dramatic difference in electrochemical performance was observed. SnO_2/KB anodes exhibited a high initial discharge (Li insertion) capacity of 1098 mAh/g; however, only 534 mAh/g was delivered for the first charge (Li extraction).The Coulombic efficiency for the first cycle is only about 48.6%. In contrast, SnO_2/MSCS composite shows superior electrochemical performance as shown in Figure 4.This can be attributed to its distinct three-dimensional structure and morphology. Open pore channels in the 3D nanostructure of the composite ensure an even distribution of electrolyte in contact with the SnO_2 surface. Electrolyte can permeate into the composite in all directions thus providing quick lithium ion diffusion through the interface. The interior void space and nanorods of carbon prevent the adjacent SnO_2 from coalescing and accommodate the tremendous mechanical strain during electrochemical cycling. The initial discharge capacity of SnO_2/MSCS was 2038 mA h/g. During the first charge process (Li extraction), the SnO_2/MSCS composite exhibits a very high capacity of 1468 mAh/g (based on the SnO_2 mass), which is essentially equivalent to the theoretical capacity within experimental error. This suggests the conversion reaction of SnO_2 in the SnO_2/MSCS is nearly completely reversible. To further support our assumption, we performed cyclic voltammogram (CV) measurements of SnO_2/MSCS in the voltage range of 0.005−3 V at a scanning rate of 0.1 mV s^{-1}. The CV curves are displayed in Figure 4c. In the first cathodic scan, two reduction peaks around 0.8 and 0.05 V are clearly observed. The former can be generally attributed to the SEI layer formation, which disappeared in the following cycles.[12,15] The latter, more intense and sharp peak is known to arise from the formation of Li_xSn, as depicted in eq 2. During the first anodic scan, oxidation peaks of 0.58, 1.3, and 2.1 V were observed, which should be related to the oxidation of Sn to SnO_2. The peak at 1.3 V was quite intense, about 60% of intensity of the peak located at 0.58 V, which is much higher than reported in the literature.[32] This indicates high degree of reversibility according to eq 1.[12,15] The CV curves of the second and third cycles almost overlapped, implying excellent cyclability of the SnO_2/MSCS electrode. The redox pairs (0.05 V, 0.58 V), (0.45 V, 1.3 V) and (1.0 V, 2.1 V) were also observed in the subsequent CVs. The latter pairs are rarely present, or have very low peak intensity in the literature.[18,21,32] This strongly implies that the conversion between SnO_2 and Sn is highly reversible. The initial Coulombic efficiency has been significantly improved from less than 50% for SnO_2/KB to over 72%. The second discharge capacity decreased to 1491 mA h/g (total of 8.4 Li-ions insertion per formula unit of SnO_2), due to the completion of SEI formation of the first discharge. The

dx.doi.org/10.1021/am4021846 | ACS Appl. Mater. Interfaces 2013, 5, 7682−7687

Coulombic efficiency of the electrode increased to 96% in the second cycle and beyond 98% in the subsequent cycles. It indicates that the formed SEI film remained intact after the first discharge SEI surface reactions were completed. Both charge and discharge capacities remained nearly constant for subsequent cycles with little fading over 15 cycles. The discharge capacity of the 15th cycle is 1318 mA h/g (92% of the initial reversible capacity), which is considerably better than previously reported results.[10−14,21,22,34,35] Even after 30 cycles, 1145 mA h/g capacity remained.

Previous reports concerning SnO_2−GNS or SnO_2−CNT composite show mass loading of 0.9 mg/cm^2 and 0.79 mg/cm^2, respectively.[12,21] For SnO_2/MSCS composite, the mass loading of electrode materials is about 3 mg/cm^2 for the 25 μm thickness electrode, which is significant higher than those reports. The volumetric capacity of the SnO_2/MSCS is calculated to be ∼1440 mA h/cm^3 (see the Supporting Information for calculation details), which is almost five times higher in comparison to previous literature reports concerning SnO_2−CNT composite (262 mA h/cm^3).[21] Therefore, the spherical morphology and submicrometer size of MSCS/SnO_2 composite is beneficial for obtaining high volumetric capacity.

The spherical shape of SnO_2/MSCS composite (see Figure S3 in the Supporting Information) was well-maintained after cycling and no obvious morphology change was observed after 30 cycles. It is evident that SnO_2/MSCS composites can effectively accommodate the volume change and alleviate strain during the insertion/extraction reaction, thus retaining structural integrity. To further prove that the unique nanoarchitecture of starburst carbon has a very positive contribution to the superior electrochemical performance of the composite, we carried out an additional control experiments by using a simple mixture of SnO_2/MSCS (SMix) sample, which contained 80 wt % MSCS with 20 wt % SnO_2 nanoparticles. This was prepared by physically mixing the components with a planetary centrifugal mixer. At a current density of 80 mA/g, SMix electrode exhibited an initial discharge and charge capacity of 1870 and 1133 mA h/g, respectively, with a low Coulombic efficiency of 35% because of a very large first irreversible capacity, which may related to SEI formation. Although the Coulombic efficiency of the electrode increased to 91% in the second cycle, it only increased slightly during subsequent cycles. After 30 cycles, the efficiency is still approximately 95−97%. This may suggest stable SEI formation was not complete. Also, the capacity of SMix electrode faded very quickly, as only 64% capacity remained at the 15th cycle. After 30 cycles, only 435 mAh/g reversible capacity remained (see Figures S5 and S6c in the Supporting Information). This result is expected, as SnO_2 nanoparticles cannot be fully incorporated into the structure by simple mixing, SnO_2 nanoparticles outside the MSCS cannot be protected by the structure, leading to pulverization and agglomeration during cycling, which causes severe capacity fading. The open pore channels in MSCS allow for a high amount of metal or metal oxide incorporation, and the interior void space of MSCS is very helpful to accommodate large strain due to volume expansion from the materials during electrochemical cycling. The unique nanostructure of MSCS also provided a confined environment to restrict the mobility of SnO_2 particles. The large surface areas available from MSCS also contribute positively to lithium-ion diffusion. Therefore, exceptional high capacity and capacity retention of battery anodes can be achieved with this new anode composite in our fresh approach. In addition, very high reversible reactions occur during delithiation and the solid-electrolyte interphase (SEI) layer may likely be formed primarily on the MSCS, which protects the metal/metal oxide from further reaction with the electrolyte, leading to significantly reduced first capacity loss.

3. CONCLUSION

In summary, a smart design of monodispersed SnO_2/MSCS composite with very high content of SnO_2 can be achieved by a simple infiltration procedure. The synergistic effects of the unique nanoarchitecture of MSCS and ultrafine size of SnO_2 nanoparticle endowed the composite with superior electrochemical performance. Because of the high density of the composite from monodispersed submicrometer spherical morphology, an extremely high reversible lithium storage capacity, very close to the theoretical capacity (1491 mA h/g) can be achieved. The combination of exceptional capacity (both gravimetric and volumetric capacity) and high Coulombic efficiency with a conventional binder (PVDF) was achieved for the first time. This may open a new area for the development of practical tin-based electrodes in lithium batteries. This general approach may also be applied to other metal alloy or conversion compounds for high-performance Li ion electrodes and could be applicable to other nanoscale building blocks and compositions beyond metal oxides.

■ ASSOCIATED CONTENT

Ⓢ Supporting Information

Experimental details and additional experimental data including TEM images, SEM image of a cycled electrode, calculation of filling degree of SnO_2/MSCS, N_2 adsorption−desorption isotherms, and plots of Coulombic efficiency upon charge/discharge are provided. This material is available free of charge via the Internet at http://pubs.acs.org.

■ AUTHOR INFORMATION

Corresponding Author

*E-mail: jiajunchen03@yahoo.com or jack.chen@tema.toyota.com (J.C.); kazuhisa.yano@tema.toyota.com (K.Y.). Fax: 734-995-2549 (J.C. and K.Y.). Phone: 734-995-5313 (J.C.); 734-995-1002 (K.Y.).

Notes

The authors declare no competing financial interest.

■ ACKNOWLEDGMENTS

The authors are very grateful to Dr. Songtao Wu for help acquiring SEM images and assistance of nitrogen adsorption and desorption isotherms experiments; Dr. Xudong Fan for TEM analysis; and Dr. Fuminori Mizuno, Dr. Paul Fanson, and Takashi Kuzuya for useful comments about the manuscript.

■ REFERENCES

(1) Whittingham, M. S. *Chem. Rev.* **2004**, *104* (10), 4271−4301.
(2) Chen, J. *Materials* **2013**, *6* (1), 156−183.
(3) Su, X.; Wu, Q.; Zhan, X.; Wu, J.; Wei, S.; Guo, Z. *J. Mater. Sci.* **2012**, *47* (6), 2519−2534.
(4) Yang, S.; Zavalij, P. Y.; Whittingham, M. S. *Electrochem. Commun.* **2003**, *5* (7), 587−590.
(5) Fan, Q.; Chupas, P. J.; Whittingham, M. S. *Electrochem. Solid-State Lett.* **2007**, *10* (12), A274−A278.
(6) Lou, X. W.; Wang, Y.; Yuan, C.; Lee, J. Y.; Archer, L. A. *Adv. Mater.* **2006**, *18* (17), 2325−2329.

(7) Wang, Z.; Luan, D.; Boey, F. Y. C.; Lou, X. W. *J. Am. Chem. Soc.* **2011**, *133* (13), 4738−4741.
(8) Kim, C.; Noh, M.; Choi, M.; Cho, J.; Park, B. *Chem. Mater.* **2005**, *17* (12), 3297−3301.
(9) Wu, H. B.; Chen, J. S.; Lou, X. W.; Hng, H. H. *J. Phys. Chem. C* **2011**, *115* (50), 24605−24610.
(10) Paek, S.-M.; Yoo, E.; Honma, I. *Nano Lett.* **2008**, *9* (1), 72−75.
(11) Wang, X.; Cao, X.; Bourgeois, L.; Guan, H.; Chen, S.; Zhong, Y.; Tang, D.-M.; Li, H.; Zhai, T.; Li, L.; Bando, Y.; Golberg, D. *Adv. Funct. Mater.* **2012**, *22* (13), 2682−2690.
(12) Li, X.; Meng, X.; Liu, J.; Geng, D.; Zhang, Y.; Banis, M. N.; Li, Y.; Yang, J.; Li, R.; Sun, X.; Cai, M.; Verbrugge, M. W. *Adv. Funct. Mater.* **2012**, *22* (8), 1647−1654.
(13) Wang, D.; Kou, R.; Choi, D.; Yang, Z.; Nie, Z.; Li, J.; Saraf, L. V.; Hu, D.; Zhang, J.; Graff, G. L.; Liu, J.; Pope, M. A.; Aksay, I. A. *ACS Nano* **2010**, *4* (3), 1587−1595.
(14) Luo, B.; Wang, B.; Li, X.; Jia, Y.; Liang, M.; Zhi, L. *Adv. Mater.* **2012**, *24* (26), 3538−3543.
(15) Chen, Z.; Zhou, M.; Cao, Y.; Ai, X.; Yang, H.; Liu, J. *Advanced Energy Materials* **2012**, *2* (1), 95−102.
(16) Liang, J.; Wei, W.; Zhong, D.; Yang, Q.; Li, L.; Guo, L. *ACS Appl. Mater. Interfaces* **2011**, *4* (1), 454−459.
(17) Zhang, L.-S.; Jiang, L.-Y.; Yan, H.-J.; Wang, W. D.; Wang, W.; Song, W.-G.; Guo, Y.-G.; Wan, L.-J. *J. Mater. Chem.* **2010**, *20* (26), 5462−5467.
(18) Ding, S.; Luan, D.; Boey, F. Y. C.; Chen, J. S.; Lou, X. W. *Chem. Commun.* **2011**, *47* (25), 7155−7157.
(19) Chen, J. J.; Whittingham, M. S. *Electrochem. Commun.* **2006**, *8* (5), 855−858.
(20) Chen, J. *Rec. Pat. Nanotechnol.* **2013**, *7* (1), 2−12.
(21) Ren, J.; Yang, J.; Abouimrane, A.; Wang, D.; Amine, K. *J. Power Sources* **2011**, *196* (20), 8701−8705.
(22) Noerochim, L.; Wang, J.-Z.; Chou, S.-L.; Wexler, D.; Liu, H.-K. *Carbon* **2012**, *50* (3), 1289−1297.
(23) Derrien, G.; Hassoun, J.; Panero, S.; Scrosati, B. *Adv. Mater.* **2007**, *19* (17), 2336−2340.
(24) Hassoun, J.; Derrien, G.; Panero, S.; Scrosati, B. *Adv. Mater.* **2008**, *20* (16), 3169−3175.
(25) Oh, S. W.; Bang, H. J.; Myung, S.-T.; Bae, Y. C.; Lee, S.-M.; Sun, Y.-K. *J. Electrochem. Soc.* **2008**, *155* (6), A414−A420.
(26) Oh, S. W.; Myung, S.-T.; Oh, S.-M.; Oh, K. H.; Amine, K.; Scrosati, B.; Sun, Y.-K. *Adv. Mater.* **2010**, *22* (43), 4842−4845.
(27) Oh, S.-M.; Myung, S.-T.; Park, J. B.; Scrosati, B.; Amine, K.; Sun, Y.-K. *Angew. Chem., Int. Ed.* **2012**, *51* (8), 1853−1856.
(28) Nakamura, T.; Yamada, Y.; Yano, K. *Microporous Mesoporous Mater.* **2009**, *117* (1−2), 478−485.
(29) Yamada, Y.; Nakamura, T.; Yano, K. *Chem. Lett.* **2008**, *37* (3), 378−379.
(30) Goodman, M. D.; Arpin, K. A.; Mihi, A.; Tatsuda, N.; Yano, K.; Braun, P. V. *Adv. Opt. Mater.* **2013**, *1* (4), 300−304.
(31) Bolzan, A. A.; Fong, C.; Kennedy, B. J.; Howard, C. J. *Acta Crystallogr., Sect. B* **1997**, *53* (3), 373−380.
(32) Di Lupo, F.; Gerbaldi, C.; Meligrana, G.; Bodoardo, S.; Penazzi, N. *Int. J. Electrochem. Sci.* **2011**, *6* (8), 3580−3593.
(33) Tatsuda, N.; Nakamura, T.; Yamamoto, D.; Yamazaki, T.; Shimada, T.; Inoue, H.; Yano, K. *Chem. Mater.* **2009**, *21* (21), 5252−5257.
(34) Park, M.-S.; Kang, Y.-M.; Wang, G.-X.; Dou, S.-X.; Liu, H.-K. *Adv. Funct. Mater.* **2008**, *18* (3), 455−461.
(35) Wen, Z.; Wang, Q.; Zhang, Q.; Li, J. *Adv. Funct. Mater.* **2007**, *17* (15), 2772−2778.